

Article

TGA-FTIR Analysis of Biomass Samples Based on the Thermal Decomposition Behavior of Hemicellulose, Cellulose, and Lignin

Esin Apaydın Varol *  and Ülker Mutlu

Department of Chemical Engineering, Faculty of Engineering, Eskisehir Technical University, 26555 Eskişehir, Turkey

* Correspondence: eapaydin@eskisehir.edu.tr; Tel.: +90-222-213-8196

Abstract: The slow pyrolysis characteristics of lignocellulosic biomass and its three major components via a Thermogravimetric Analyzer coupled with a Fourier Transform Infrared Spectrometer (TGA-FTIR) was studied. Different compositions and ratios of cellulose, hemicellulose, and lignin, olive pomace, sunflower waste, and pinecone were selected. The main decomposition temperature ranges of xylose (hemicellulose) and lignin showed a broad range between 173–690 and 170–835 °C, respectively, whereas that of cellulose was detected to be 291–395 °C. All biomass samples presented a three-stage pyrolysis model that is explained by the superposition of the weight losses of major components. Simultaneous FTIR analysis of the evolved gases demonstrated that the greater the cellulose and hemicellulose contents, the higher the CO and CO₂ concentrations. Chemical kinetics were computed with the Coats–Redfern model. The activation energy required for the initiation of the thermal decomposition of biomass samples is in the range of 53–94 kJ/mol. Moreover, the product yields of all samples were determined via laboratory-scale pyrolysis. Pyrolytic oil and char yields were determined to be between 18.9–32.4 wt.% and 26.6–31.2 wt.%, respectively, at 550 °C final temperature for the biomass samples. It is concluded that the bio-oil yield was not only controlled by the cellulose content but also affected by the presence of n-hexane soluble (oil) fraction as well as inorganics.

Keywords: olive pomace; pinecone; pyrolysis; sunflower waste; TGA-FTIR



Citation: Apaydın Varol, E.; Mutlu, Ü. TGA-FTIR Analysis of Biomass Samples Based on the Thermal Decomposition Behavior of Hemicellulose, Cellulose, and Lignin.

Energies **2023**, *16*, 3674. <https://doi.org/10.3390/en16093674>

Academic Editor: Tiit Lukk

Received: 30 March 2023

Revised: 18 April 2023

Accepted: 21 April 2023

Published: 25 April 2023



Copyright: © 2023 by the authors. Licensee MDPI, Basel, Switzerland. This article is an open access article distributed under the terms and conditions of the Creative Commons Attribution (CC BY) license (<https://creativecommons.org/licenses/by/4.0/>).

1. Introduction

In recent years, global environmental problems related to the consumption of fossil resources have been experienced due to the increasing industrialization and population. Several renewable energy technologies have been extensively conducted to life to replace fossil fuel utilization [1,2]. Biomass, as a carbon-neutral source, seems to be one of the most promising candidates for the production of biofuels that could substitute conventional fuels and reduce CO₂ and NO_x emissions. Among the possible biomass conversion processes, thermochemical technologies are the most suitable ones as they can provide synthetic fuels with high calorific value. The pyrolysis process is a thermochemical conversion method that produces biofuel, the yield and composition of which are dependent on both the pyrolysis conditions and the type of biomass [3,4]. The pyrolysis behavior of biomass is strongly related to its three major components: hemicellulose, cellulose, and lignin, together with extractives and ash.

Cellulose, which can be symbolized as (C₆H₁₀O₅)_n, is the most abundant natural organic polymer with a high molecular weight of 300,000 and 500,000. Typically, the cellulose content varies between 30–50 wt.% depending on the type of biomass [5]. Hemicellulose is the second major chemical constituent comprising 10 to 40% of the mass of biomass and is chemically related to cellulose with a heterogeneous structure [5,6]. It is a mixture of various polymerized monosaccharides built up of different hexoses (C₆-sugars) and

pentoses (C5-sugars). The aromatic polymer lignin is the third major component of biomass, accounting for 23–33% of the mass of softwood and 16–25% of the mass of hardwood [5]. It provides mechanical support to the plant during its growth. Due to having an amorphous cross-linked resin with no exact structure, lignin is composed of benzene rings joined with methoxy-, hydroxy-, and propyl- groups. In addition to these major components, biomass also contains inorganics, mainly K, Na, Ca, Si, and others, that can be observed through the ash. Organic extractives are the last group of constituents of biomass, including fats, waxes, alkaloids, proteins, phenolics, simple sugars, pectins, mucilages, gums, resins, terpenes, starches, glycosides, saponins, and essential oils. In addition, biomass has a substantial amount of water, both in free and bound form. The lignocellulosic complex holds water in the form of fibers, vessels, and other anatomical parts [7–9].

Thermal decomposition behavior of the major components of biomass has importance on the degradation of biomass. In the last decade, researchers have studied the effect of constituents on pyrolysis and also on the chemical and physical properties of bio-oil and biochar [10–12]. Chen et al. examined the possible reaction pathways and kinetics of cellulose, hemicellulose, and lignin and the pyrolysis product characterization [13]. Zhu and Zhong reported the activation energy and pre-exponential factor as the kinetic parameters for the biomass constituents [14]. The effect of different pyrolysis conditions on the lignocellulosic biomass pyrolysis yield and quality was studied to investigate the environmental and economic aspects of pyrolysis by Yogalakshmi et al. [15]. On the other hand, the pyrolytic behavior of several biomass samples has been studied since the last quarter of the 20th century [16–18]. Pyrolysis (slow or fast) kinetics and/or product yields and product characterization via several instrumental techniques have been published [19–21]. Table 1 summarizes the new developments in biomass pyrolysis, where the effects of several parameters on the pyrolysis characteristics of lignocellulosic materials were reported. In addition, studies published in recent years on biomass pyrolysis include artificial neural networks or computer-based modeling applications, which require a large number of data to be used in validating the results. On the other hand, plenty of literature is available on the comparison and characterization of slow pyrolysis yields of both the constituents and different biomass samples and their decomposition behaviors.

The novelty of this work is to gain pyrolysis data to understand the complex relationship between biomass composition and pyrolysis behavior. While previous studies have investigated the pyrolysis behavior of various biomass samples, the inclusion of the effect of biomass constituents has the potential to provide insights into the factors that influence the product yields of slow pyrolysis. Overall, this study focuses on the effect of biomass constituents on the pyrolysis behavior of different biomass samples, which has the potential to contribute data to the literature for the development of more efficient and sustainable biomass conversion technologies and for their possible usage in artificial neural network studies.

In this context, the present work aims to investigate the pyrolysis characteristics of selected biomass samples and biomass constituents using both a fixed bed batch-type reactor and a thermogravimetric analyzer coupled with a Fourier-transform infrared spectrometer (TG-FTIR). To accomplish these objectives, olive pomace as an industrial by-product, sunflower waste as an agricultural biomass, and pinecone as a forestry biomass have been selected for the experimental studies. The tendency of bio-oil, char, and gas product formation as a consequence of biomass pyrolysis was enlightened through the pyrolytic characteristics of hemicellulose, cellulose, and lignin.

Table 1. Selected studies about the comparison of biomass types and characteristics and pyrolysis conditions on the pyrolysis product yields.

Biomass Type	Holocellulose Content (wt. %)	Lignin Content (wt. %)	Pyrolysis Conditions	Main Objectives	Ref.
Oak wood chips	59.07	25.41	Lab-scale cylindrical pyrolyzer H.R. *: 5–100 °C/min N ₂ flow: 50–300 mL/min Temperature: 400–800 °C	Effects of pyrolysis conditions on the product yields and quality	[22]
Pine sawdust	69.97	26.67	Laboratory scale pyrolyzer H.R.: 10 °C/min N ₂ Flow rate: 50–200 cm ³ /min	The pyrolysis behavior of real and synthetic biomass samples was compared with predicted characteristics.	[23]
Sunflower husk	69.46	28.48	Temperature: 350–575 °C		
Pine sawdust	71.27	10.55	Semi-batch reactor H.R.: 50–120 °C/min	The effect of biomass bed thickness and distance between successive beds on pyrolytic product yield and characterization	[24,25]
Sal sawdust	66.95	11.18	N ₂ Flow rate: 100 cm ³ /min		
Areca nut husk	65.79	13.27	Temperature: 400–600 °C		
Cornstalk	64	15	TGA experiments H.R.: 20 °C/min	Effect of the correlation between the cellulose and lignin content on the reaction conversion	[26]
Larch bark	59	35	N ₂ flow rate: 120 mL/min		
Bagasse	74	90	Temperature: 900 °C		
Pine needles	N.A. **	N.A.	Laboratory scale pyrolyzer H.R.: 10–50 °C/min N ₂ Flow rate: 50–200 cm ³ /min	Effects of nitrogen flow rate, particle size, and final temperature on the product yields and characteristics of bio-oil and char	[27]
			Temperature: 350–650 °C		
33 biomass materials	N.A.	N.A.	Microwave-enhanced fast pyrolysis system H.R.: 1.5–50 °C/s N ₂ flow rate: 0.9 L/min	The various effects of biomass and pyrolysis conditions on microwave-enhanced fast pyrolysis product yields and qualities	[27]
			Temperatures: 500 °C		
Miscanthus	76.9	12.2	MATLAB R2015b	Derivation of a mathematical model to predict the production of biochar, flue gas, and tar under different pyrolysis conditions	[28]
Bamboo	69	23.2	Temperature: 200–1000 °C		
482 lignocellulosic samples	N.A.	N.A.	Artificial neural networks	The prediction of the solid, liquid, and gas yields from pyrolysis processes	[29]

* H.R.—Heating Rate, ** N.A.—not available.

2. Materials and Methods

2.1. Materials

Hemicellulose (xylose, Acros Organics, Branchburg, NJ, USA), cellulose (Sigma Aldrich, St. Louis, MO, USA), and lignin (Sigma Aldrich, USA) were used to investigate their function in biomass pyrolysis. Olive oil residue-olive pomace (Aydın, Turkey), sunflower waste (Bursa, Turkey), and pinecone (Aydın, Turkey) were selected as the biomass samples since their compositions are different. All biomass samples were air-dried and ground to obtain a uniform particle size of $1.25 < D_p < 0.625$ mm.

Biomass samples were characterized in terms of proximate and ultimate analyses, acid insoluble lignin, holocellulose, extractive, and n-hexane soluble fraction (oil content) determination according to standard test methods given in Table 2.

Table 2. Properties of biomass components and selected samples.

Analysis (wt.%)	Method	Xylose	Cellulose	Lignin	Pinecone	Olive Pomace	Sunflower Waste
Moisture	ASTMD 2016-74	1.44	4.97	9.35	9.23	6.31	8.19
Ash	ASTMD 1102-84	~0	~0	33.46	1.20	4.85	11.20
Volatile matter	ASTME 897-82	91.02	91.25	40.05	71.05	70.99	67.43
Fixed carbon	From difference	7.54	3.78	17.14	18.52	17.85	13.18
Holocellulose	TS 324	-	-	-	57.12	55.02	64.58
Oil	TS 769	-	-	-	2.35	5.78	4.50
Extractives	ASTMD 1105-84	-	-	-	9.70	5.02	9.75
Lignin	ASTMD 1106-84	-	-	-	29.50	34.04	20.22

2.2. Thermal Decomposition Behaviour-TGA-FTIR Analysis

The thermal decomposition behavior of the samples was determined using a Setaram Labsys Evo Thermogravimetric Analyzer, and the sample weight losses were recorded as a function of temperature and time. Prior to the experiments, a blank test was conducted. Afterward, for each experiment, 10 ± 0.5 mg of the sample was weighed in a 100 μ L alumina crucible without a lid. The heating program was applied as follows: a heating rate of 10 $^{\circ}$ C/min in the temperature range from 25 $^{\circ}$ C to 1000 $^{\circ}$ C with a nitrogen flow at a rate of 20 mL/min to maintain an inert atmosphere. All experiments were carried out at least three times to check the accuracy and precision of the data and to decrease the experimental errors.

During the thermal decomposition, the evolved gases were simultaneously analyzed by Thermo Nicolet IZ 10 FT-IR spectrometer. The gases were transferred from the TGA furnace to the FTIR gas cell, where the transfer line and the gas cell were kept at 225 and 250 $^{\circ}$ C, respectively, to avoid condensation of the gases. IR spectra were recorded between 4000–700 cm^{-1} at a resolution of 4 cm^{-1} with 32 scans. The OMNIC software program was used to obtain three-dimensional spectra, Gram-Schmidt curves, and chemigrams to identify each functional group with time and temperature.

2.3. Pyrolysis Kinetics Modeling

The data obtained from TGA was used to identify pyrolysis kinetics for biomass components and selected samples. One of the common non-isothermal model-fitting techniques, where the degree of the reaction order is needed to be assumed, and the Taylor series expansion is used for the arrangement of the integral, is known as the Coats and Redfern (CR) equation (Equation (1))

$$\ln \left[\frac{-\ln(1-\alpha)}{T^2} \right] = \ln \left[\frac{AR}{\beta E_a} \left(1 - \frac{2RT}{E_a} \right) \right] - \frac{E_a}{RT} \quad (1)$$

where T is the absolute temperature (K), A is the pre-exponential factor (1/s), E_a is the activation energy (kJ/mol), R is the ideal gas constant (8.3144 J/mol.K), and α is the degree of conversion that is expressed as:

$$\alpha = \frac{w_i - w}{w_i - w_f} \quad (2)$$

where w_i is the initial mass of the sample, w_f is the final mass and w is the mass at any time t .

Equation (1) can be simplified by assuming usual values of E_a between 80–260 kJ/mol for $2RT/E_a \ll 1$ to get the following equation:

$$\ln\left(\frac{g(\alpha)}{T^2}\right) = \ln\left(\frac{AR}{\beta E_a}\right) - \frac{E_a}{RT} \quad (3)$$

Here, $g(\alpha)$ is the integrated reaction model, which is expressed in Equation (4) and β is the heating rate (K/s). Plotting $\ln(g(\alpha)/T^2)$ versus $1/T$ using single heating rate data yields a straight line. E_a and A can be obtained from the slope of the line, E_a/R , and its intercept, $\ln(AR/E_a)$.

$$g(\alpha) = \int_0^\alpha \frac{d\alpha}{f(\alpha)} = \frac{A}{\beta} \int_0^{T_\alpha} \exp\left(\frac{-E_a}{RT}\right) dT \quad (4)$$

where T_α is the temperature at conversion α and $f(\alpha)$ is the function stating the dependence of the reaction rate on the conversion. To able to solve this integral, E_a/RT is defined as x , and equation becomes:

$$g(\alpha) = \frac{AE_a}{\beta R} \int_\alpha^\infty \frac{\exp^{-x}}{x^2} = \frac{AE_a}{\beta R} p(x) \quad (5)$$

The temperature integral, $p(x)$, cannot be solved analytically. However, the Coats–Redfern method approximates $p(x)$ using a Taylor series expansion to yield Equation (3) [30,31].

2.4. Laboratory Scale Pyrolysis Studies

Slow pyrolysis experiments were performed in a fixed-bed reactor having a volume of 400 cm³, details of which were given elsewhere [32,33]. Temperature measurements were carried out using a thermocouple placed on the bed above the sample. The experimental conditions for the slow pyrolysis system were as follows: pyrolysis temperature ranged from room temperature to 550 °C, heating rate of 10 °C/min, and nitrogen flow rate of 100 cm³/min. The volatiles formed during pyrolysis were immediately cooled and condensed by an ice bath maintained at around 0 °C. The bio-oil was then washed with dichloromethane from the collecting traps, and the solvent was removed by a rotary evaporator. The condensable fractions also contained a considerable amount of water which was further separated by a separation funnel. The amounts of bio-oil and water were determined, and bio-oil yields were calculated on a dry ash-free basis as follows:

$$\text{Bio-oil yield (wt.\%)} = m_{\text{oil}} / (m_i (1 - x_{\text{ash}} - x_{\text{moisture}})) \quad (6)$$

$$\text{Char yield (wt.\%)} = m_{\text{char}} / (m_i (1 - x_{\text{ash}} - x_{\text{moisture}})) \quad (7)$$

$$\text{Water yield (wt.\%)} = m_{\text{water}} / (m_i (1 - x_{\text{ash}} - x_{\text{moisture}})) \quad (8)$$

$$\text{Gas Yield (wt.\%)} = 100 - (\text{Bio-oil yield} + \text{Char yield} + \text{Water yield}) \quad (9)$$

where, m_{oil} , m_{char} , and m_{water} are the amounts of bio-oil, char, and water formed in grams, m_i is the initial amount of sample in grams, and x_{ash} and $x_{moisture}$ are the fractions of ash and moisture in the sample.

All experiments were performed at least three times, and the average yields with an experimental measurement error of less than $\pm 0.5\%$ were given in this study.

3. Results and Discussion

3.1. Properties and Thermal Decomposition Behavior of Biomass Components and Selected Samples

The proximate analysis results of biomass constituents and selected samples are given in Table 2. Lignin, as the highly aromatic structured component, has the highest amount of fixed carbon with 17.14 wt.%, whereas xylose and cellulose have significantly higher amounts of volatile matter contents, more than 90 wt.%. Therefore, during the pyrolysis of lignocellulosic biomass, lignin shows resistance to relatively higher temperatures due to the requirement of high energy for the breakage of the double bonds existing in its structure.

For the biomass samples, similar volatile matter and moisture contents are observed (Table 2). The fixed carbon content of sunflower waste is 13.18 wt.%, which is relatively lower than that of the other biomass samples due to its high ash content of 11.20 wt.%. The effect of ash (inorganics) on pyrolysis has been investigated previously by researchers, and it is mainly mentioned that the presence of ash has a strong effect on the pyrolysis and gasification of the char since inorganic species act as a catalyst during thermal decomposition [34,35]. On the other hand, when scale-up processes are required, the presence of high amounts of ash is problematic due to its accumulation in the pyrolysis/gasification reactors, and also extra equipment should be installed in the process to separate ash from the gas product.

Table 2 lists the constituents of biomass samples. Holocellulose is referred to the total amount of cellulose and hemicelluloses in the lignocellulosic biomass [36]. All samples comprised of holocellulose more than 55 wt.%, denoting that there is a remarkable volatile fraction in their structure. The sunflower waste contains the highest amount of holocellulose (64.58 wt.%) and the minimum amount of lignin (20.22 wt.%). The n-hexane soluble extractives, in other words, oil fraction, achieved their highest value for the olive pomace sample with an amount of 5.78 wt.%.

After the preliminary analysis, FT-IR spectra were taken to determine the functional groups of the biomass components and raw materials. FT-IR spectra are given in Figure 1, and the results are given in Table 3. It is not surprising to see that all samples presented similar spectra and had many common functional groups (Figure 1a). The spectra can be examined in three regions: the first one between $3400\text{--}2800\text{ cm}^{-1}$ and the second between $1800\text{--}100\text{ cm}^{-1}$, while the last one is the fingerprint region below 900 cm^{-1} . In this manner, the broad stretching vibration band seen at $3400\text{--}3000\text{ cm}^{-1}$ is attributed to O-H groups, and the medium and weak band at around $2800\text{--}3000\text{ cm}^{-1}$ is indicative of asymmetric and symmetric stretching C-H vibrations in xylose, cellulose, and lignin structures. The bands between $1740\text{--}1510\text{ cm}^{-1}$ are due to olefinic C=C and C=O vibrations in aromatic structures. The bending vibrations $1460\text{--}1325$ and $900\text{--}750\text{ cm}^{-1}$ are assigned to C-H, whereas the strong C-O stretching vibrations are observed between $1280\text{--}1030\text{ cm}^{-1}$ [37,38].

Hydroxyl group stretching vibrations arising from the polysaccharides are one of the similar bands for all biomass samples since they all include cellulose. In addition, the second indicative of polysaccharides, i.e., C-H vibrations around 2900 cm^{-1} , is observed not only for cellulose but also for all samples. The appearance of C-O stretching vibration bands ($1200\text{--}1000\text{ cm}^{-1}$) that belong to the main glucosic structure of cellulose is detected for all biomass samples. Since lignin has a three-dimensional phenolic and polymeric structure composed of phenyl propane, it also contributes to the C-H and O-H vibrations. In addition, being the only aromatic component in the biomass samples, its presence is supported by the intense C=C vibrational band seen between 1620 and 1510 cm^{-1} [39]. The FTIR spectra of all biomass samples resemble each other due to having similar vibrations arising from a similar structure.

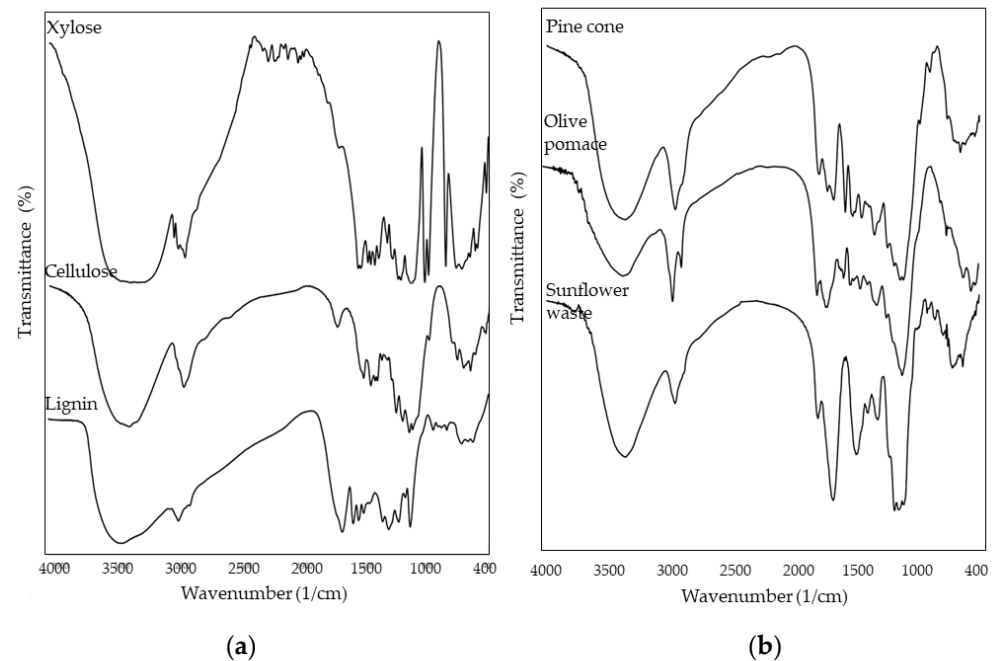


Figure 1. FT-IR spectra of (a) biomass constituents and (b) biomass samples.

Table 3. FT-IR analysis of biomass constituents and selected samples.

Wave number (1/cm)	Functional Groups *	Assignment	Xylose	Cellulose	Lignin	Pinecone	Olive Pomace	Sunflower Waste
3400–3000	O-H (ν)	Alcohol, phenol, carboxylic acids	3331	3346	3400	3345	3336	3340
3000–2800	C-H (ν)	Alkanes, alkenes	2978 2889	2900	2935	2928	2925 2854	2928
1740–1600	C=O (ν)	Ketones, aldehydes	1632	-	1596	1734 1663	1732 1660	1737
1620–1510	C=C (ν)	Olefinics, aromatics	-	-	1506	1611 1511	1538 1516	1612
1460–1325	C-H (δ)	Aliphatic	1476 1395 1373 1312	1432 1372 1336	1421 1374	1454 1379	1455 1378	1423 1323
1280–1030	C-O (ν)	Alcohol, phenol, ester, ether	1150 1128 1040	1165 1113 1032	1266 1217 1135 1042	1272 1163	1244 1163 1033	1243 1101
900–750	C-H (δ)	Aromatics	904 760	897	856 743	895	755	833 768

* ν —stretching vibrations; δ —bending vibrations.

TG and dTG curves representing the thermal decomposition behavior of biomass constituents (xylose (in place of hemicellulose), cellulose, and lignin) and selected samples are given in Figures 2 and 3. In addition, Table 4 lists the results of the TGA analysis in detail. Prior to investigating the pyrolytic performance of biomass samples, it is beneficial to completely understand the decomposition pathways of the constituents.

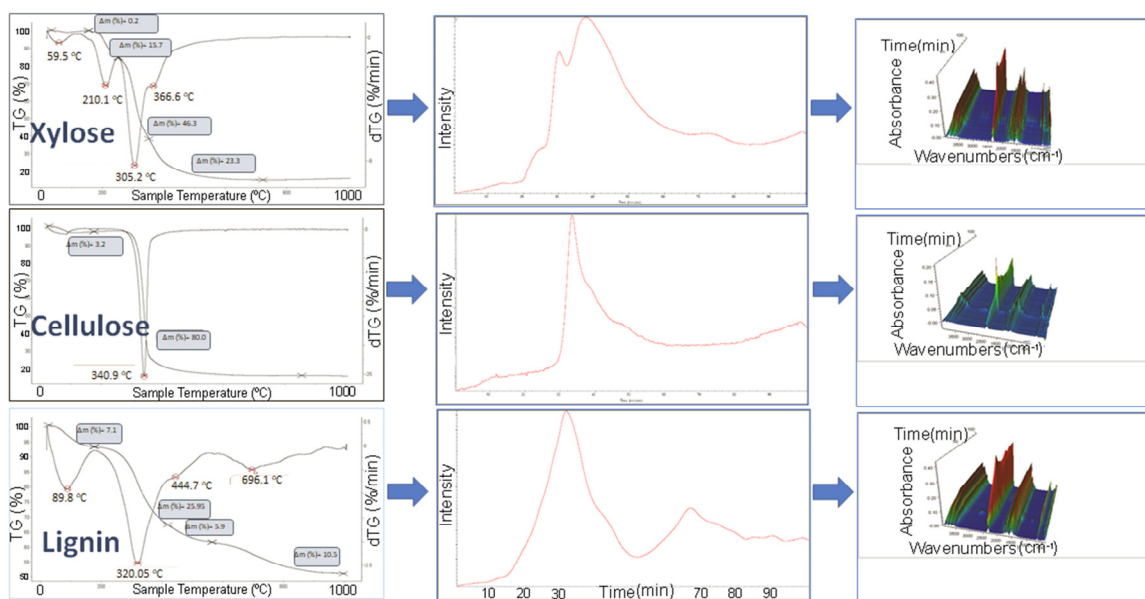


Figure 2. TGA-FTIR analysis of biomass constituents.

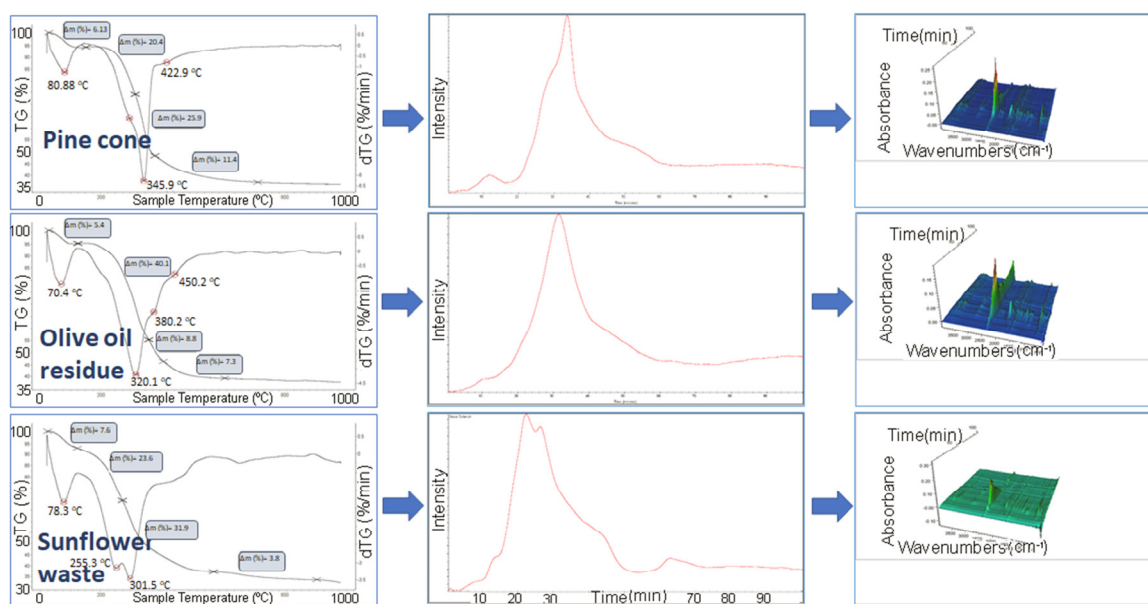


Figure 3. TGA-FTIR analysis of biomass samples.

Table 4. TGA results of biomass components and selected samples.

Sample	Moisture Release		1. Stage		2. Stage		3. Stage		Solid Residue at 1000 °C (%)
	T Range (°C)	Mass Loss (%)	T Range (°C)	Mass Loss (%)	T Range (°C)	Mass Loss (%)	T Range (°C)	Mass Loss (%)	
Xylose	25–130	0.17	173–249	15.74	258–355	46.31	360–645	23.25	14.53
Cellulose	25–130	3.17	-	-	291–395	80.0	-	-	16.83
Lignin	25–100	7.12	170–420	25.96	420–495	4.35	495–835	12.05	50.52
Pinecone	25–140	6.13	210–310	20.34	310–380	25.92	380–715	11.40	36.10
Olive pomace	25–130	5.39	188–350	40.14	350–410	8.79	410–620	7.27	37.65
Sunflower waste	25–125	7.54	160–275	21.60	275–380	27.91	380–570	4.30	33.12

The differences in the chemical structures of biomass constituents result in variations in the thermal degradation styles. Xylose, as one of the main compounds in the heterocyclic structure of hemicellulose, is readily subjected to hydrolysis reactions at lower temperatures.

From Figure 2, it can be reported that the thermal decomposition of xylose starts as the former constituent at 173 °C. Neglecting the initial mass loss (0.17 wt.%) that is related to the moisture release up to 130 °C, the decomposition of xylose is completed in three stages, as seen from the dTG curve and Table 4. Due to the highly oxygenated compounds joined to a cyclic framework, less energy is required to break the bonds, and hence more than 60% of the decomposition of xylose is completed around 355 °C. The first stage occurs at a slower rate and is completed at 249 °C. Maximum weight loss is achieved during the second stage between 258 and 355 °C with an amount of 46.31 wt.%. The last decomposition stage appears as a shoulder on the dTG curve, and the decomposition of xylose is accomplished at around 645 °C where no further mass loss is observed, and the total conversion of 80.1% is achieved (Table 5). The final amount of solid residue is attained to be 14.53 wt.% for xylose.

Table 5. Analysis of the thermogravimetric curves of the biomass components and selected samples (heating rate: 10 °C/min, nitrogen flow rate: 20 mL/min, x (%) = conversion = $(m_0 - m)/m_0 \times 100$ where m_0 is the initial mass and m is the mass of the sample at a given time).

Sample	T (°C)									
	x = 10	x = 20	x = 30	x = 40	x = 50	x = 60	x = 70	x = 80	x = 90	x@1000 °C
Xylose	221	269	290	304	319	346	392	630	>1000	80.1
Cellulose	315	325	333	337	341	345	352	468	>1000	82.9
Lignin	276	330	402	687	>1000					46.7
Pinecone	262	300	327	346	371	526	>1000			63.9
Olive pomace	242	286	314	342	387	521	>1000			62.4
Sunflower waste	175	237	271	304	347	471	>1000			67.9

The second polysaccharide component, cellulose, decomposes at 291 °C after the initial weight loss of 3.17 wt.% in a temperature range of 25–130 °C, which is associated with moisture removal. The structure of cellulose is different from hemicellulose because this natural polymer is formed by glucose molecules. The decomposition of cellulose takes place in one step with a sharp decrease in weight loss and, as seen in the dTG curve, a sudden peak with a weight loss rate of 25.6%/min at 340.9 °C. The higher initialization temperature for cellulose is due to its crystalline structure. The heterocyclic glucose molecules are primarily decomposed by the cleavage of glucosidic bonds, which is accompanied by dehydration reactions. The mass loss rate of cellulose is lowered to 0.97 wt.%/min at temperatures higher than 395 °C, and the amount of solid residue remaining is obtained as 16.83 wt.% at around 520 °C. However, the third component—lignin—undergoes a gradual decomposition over a wide temperature interval between 170 and 935 °C. In contrast to xylose and cellulose, a lower amount of mass (49.5 wt.%) is decomposed at a very slow rate. The only polymeric aromatic compound among the other constituents of biomass, lignin is composed of phenylpropane units and C=C (614 kJ/mol) bonds that require approximately two folds of bond dissociation energy than C-O (358 kJ/mol), C-C (347 kJ/mol) and C-H (413 kJ/mol) bonds [40]. The maximum weight loss rate of 2.5 wt.%/min is obtained at 320 °C where the main decomposition occurs, and at temperatures over 495 °C during the third stage; the mass loss rate is lowered to ~0.5 wt.%/min. The charring reactions occurring during the last stage led to the formation of a higher amount of solid residue than that of cellulose and xylose. Similar results were also reported previously, indicating the differences in the degradation behavior of all three components of biomass [26,41–45]. In addition, although the chemical structure of lignin and xylose is significantly different, they begin to decompose at similar temperatures, around 170 °C. However, the dissimilarity in their decomposition rates explains the different reactions taking place during degradation, where that of lignin is lower and extends to higher temperatures [46].

Figure 3 represents the thermal behavior of the selected biomass samples. As seen, the mass loss and dTG curves are similar for all lignocellulosic biomass samples, and

the pyrolysis curves are in relation to the proportions of hemicellulose, cellulose, and lignin in the biomass. The initial mass loss is associated with the moisture release up to approximately 140 °C. From the mass loss percentages, it is seen that initial mass losses are 6.13, 5.39, and 7.54 for pinecone, olive pomace, and sunflower waste, respectively. Since this initial mass loss is just the vaporization of water molecules bound on the surface of the samples, it is not related to pyrolysis, and hence it is not considered a pyrolytic reaction in this study. The slight difference between TGA and ASTM results for the moisture contents of the samples might be due to the amount of material used and sampling. At temperatures over 160 °C, all samples showed three-stage pyrolysis with different temperature ranges and mass loss rates. The decomposition of the pinecone starts at 210 °C, forming a shoulder around 300 °C, which is followed by a sharp peak for the maximum mass loss rate at about 346 °C. The third stage of the decomposition is completed with a very slow rate of lower than 0.25 wt.%/min after 550 °C, leaving a 36.10 wt.% solid residue. For olive pomace, a moisture release of 5.39 wt.% is followed by the main pyrolysis stage, where 48.93 wt.% is volatilized in the temperature range of 188–410 °C. Among the biomass samples, the solid residue left from olive pomace is the highest, 37.65%. The decomposition of sunflower waste showed three peaks in the pyrolysis region, starting at about 160 °C and reaching its maximum weight loss rate at 301.5 °C with the second peak in the dTG curve. The main pyrolytic reactions are completed at around 520 °C, and the solid residue remaining at this temperature is 38.65 wt.%. In contrast to the other biomass samples, due to its high amount of ash content, sunflower waste has an extra decomposition peak at higher temperatures of between 580 and 730 °C with a weight loss of 6.43%. This last peak can be explained by the decomposition of carbon that is absorbed by the inorganics and volatilized at high temperatures. The mass loss rates and corresponding temperatures are within the ranges that have been published for several biomass feedstocks [47–52].

According to these results, since the weight loss related to the volatilization of major components occurs at temperatures lower than 600 °C, choosing a pyrolysis temperature of 550 °C is appropriate when the maximum amount of liquid and gaseous products is aimed. It can also be concluded that during the pyrolysis of biomass, the components decompose individually, forming a superposition. However, the process of pyrolysis is still complex, and the explanations of each reaction or the synergetic effects of the components are not clear yet. Nevertheless, in a general view, biomass decomposition can be divided into three main categories; namely, (i) moisture release (25–140 °C), (ii) main pyrolysis (decomposition of hemicellulose, cellulose, and lignin in a temperature range of 170–390 °C) and (iii) further pyrolysis (decomposition of lignin between 390–835 °C), consistent with previous studies [53–55].

In addition to the above explanations, it can be noted that the maximum weight loss rate temperature is affected by the distribution of biomass components. The lowest maximum temperature of 301 °C is obtained for the sunflower waste sample that has the highest amount of holocellulose as given in Table 2. In addition, pinecone with a high amount of lignin has a maximum weight loss rate temperature of 346 °C. Although olive pomace has a significant amount of lignin originating from the high percentage of stone in the solid remainder, its maximum temperature is observed to be around 320 °C, which is due to the presence of hexane-soluble oils that accelerates the devolatilization reactions and thus decreases the temperature.

Table 5 lists the typical temperatures at which 10, 20, . . . , and 90% conversion is achieved for all samples. The maximum conversion of 60% is achieved within the temperature range of between 473 and 526 °C for biomass samples revealing that the primary and secondary pyrolytic reactions are essentially complete at temperatures around 500 °C. This is an important outcome since after this temperature; conversion is very slow, and volatile formation is limited due to the charring reactions. Among the samples, sunflower waste (high holocellulose and inorganics content) degradation starts at the lowest temperature, in other words, earlier than the others. On the contrary, the conversion of the pinecone sample (high lignin content) starts at 262 °C with 10%, and nearly complete conversion (60%) is

reached at 526 °C. This conversion versus temperature (time) table is consistent with the kinetic parameters calculated from the Coats–Redfern equation, as will be described in the next sections.

3.2. TGA-FTIR Analysis of Biomass Components and Selected Samples

The Gram–Schmidt curves of the total FT-IR absorbance intensity of gaseous products released during the pyrolysis process of the samples are presented in Figures 2 and 3. A collection of linearly independent vectors can be converted into an orthonormal basis for a given vector space using the Gram–Schmidt process, and it is a common method to represent the total change in the IR signal relative to the initial state [56]. The Gram–Schmidt curves of all samples have similar temperature ranges with weight loss curves, specifically dTG curves. In other words, Gram–Schmidt curves are all consistent with the dTG. The temperature obtained from dTG data, at which the highest conversion rate is achieved, is also delivered from the Gram–Schmidt curve as the time at which the highest gas evolution is detected. For instance, during the decomposition of lignin, the third stage happened between 495 and 835 °C as a third peak in the dTG curve and similarly, a second noticeable peak is observed in the Gram–Schmidt graph between 50 and 84 min.

The three-dimensional FT-IR spectra of biomass constituents and samples that are simultaneously obtained from the TGA are also shown on the right-hand side of Figures 2 and 3. The appearance of 3d peaks begins with an increase in time (temperature). The volatile compounds are released both during the primary pyrolysis reactions and charring reactions. Because of the overlapping peaks in the FT-IR spectra, it is challenging to determine the particular volatile species with accuracy. However, the typical bands observed at specific wavelengths are effective in interpreting the evolved gases. The gaseous products are observed in the temperature range of 165–720 °C, and they are detected to be mainly CO₂, CO, CH₄, and H₂O. These evolved gases are typical for the lignocellulosic biomass pyrolysis process [57–60]. The appearance of absorbance peaks in the 3D spectra and the mass loss in the TG curves are in good agreement. The most recognizable peaks that correspond to CO₂ stretching and bending vibrations between 2250 and 2450 cm⁻¹ and between 580 and 730 cm⁻¹, respectively, are observed during the highest devolatilization reactions. IN ADDITION, the O-H vibration bands between 3900–3400 cm⁻¹ are observed from 3d spectra, revealing the fact that water is released due to the vaporization of adsorbed moisture and the dehydration reactions taking place during the primary pyrolysis stage. The other gas products are also observed from 3d spectra. However, they are better recognized from the chemigrams given in Figures 4 and 5. The chemigram produced for the wavelength region of 3200–2850 cm⁻¹ is assigned to the formation of CH₄ due to the decomposition of phenols at high temperatures. Stretching vibration bands seen around 1650–1850 cm⁻¹ are attributed to the presence of aldehydes and ketones formed during cellulose and hemicellulose pyrolysis. In addition, C-O and O-H stretching vibration bands seen around 1300–1130 cm⁻¹ and 1085–960 cm⁻¹ indicate the presence of acids (formic acid) and alcohols (methanol) [61].

The comparison of evolved gases during the pyrolysis of xylose, cellulose, and lignin yields slight differences mainly due to the changes in the reaction mechanisms. The formation of H₂O begins slowly as the heating process starts. H₂O is produced from a two-step degradation for xylose and lignin during the primary reactions, whereas cellulose decomposition yielded H₂O as the product in a single step. Since lignin contains more methyl groups, CH₄ formation through the cracking of methoxyl, methyl, and methylene groups is more detectable than the other constituents. CO₂ is the most significant product of all constituents. It is mainly produced during the initialization reactions, such as cracking and reforming of carboxyl, carbonyl, and ester groups. Lignin decomposition produced CO₂ for up to 80 min (~820 °C) due to the charring reactions occurring at these high temperatures, which is a wider range than that of cellulose and xylose. Similarly, the cracking of carbonyl and ether groups yields CO gas as the product, and it is produced in one step for cellulose pyrolysis. Xylose presents a two-step CO formation, the first one

being more intense than the second. While the evolution of CO starts around 26 and 29 min for xylose and cellulose, respectively, it is released after 52 min for lignin, as also reported by other researchers [13]. In addition to the formation of these gases, other low molecular weight hydrocarbons, such as acidic and alcoholic groups, are also released, as given in the chemigrams. However, these gases have lower intensities when compared to the others, indicating the occurrence of leading CO₂-producing reactions.

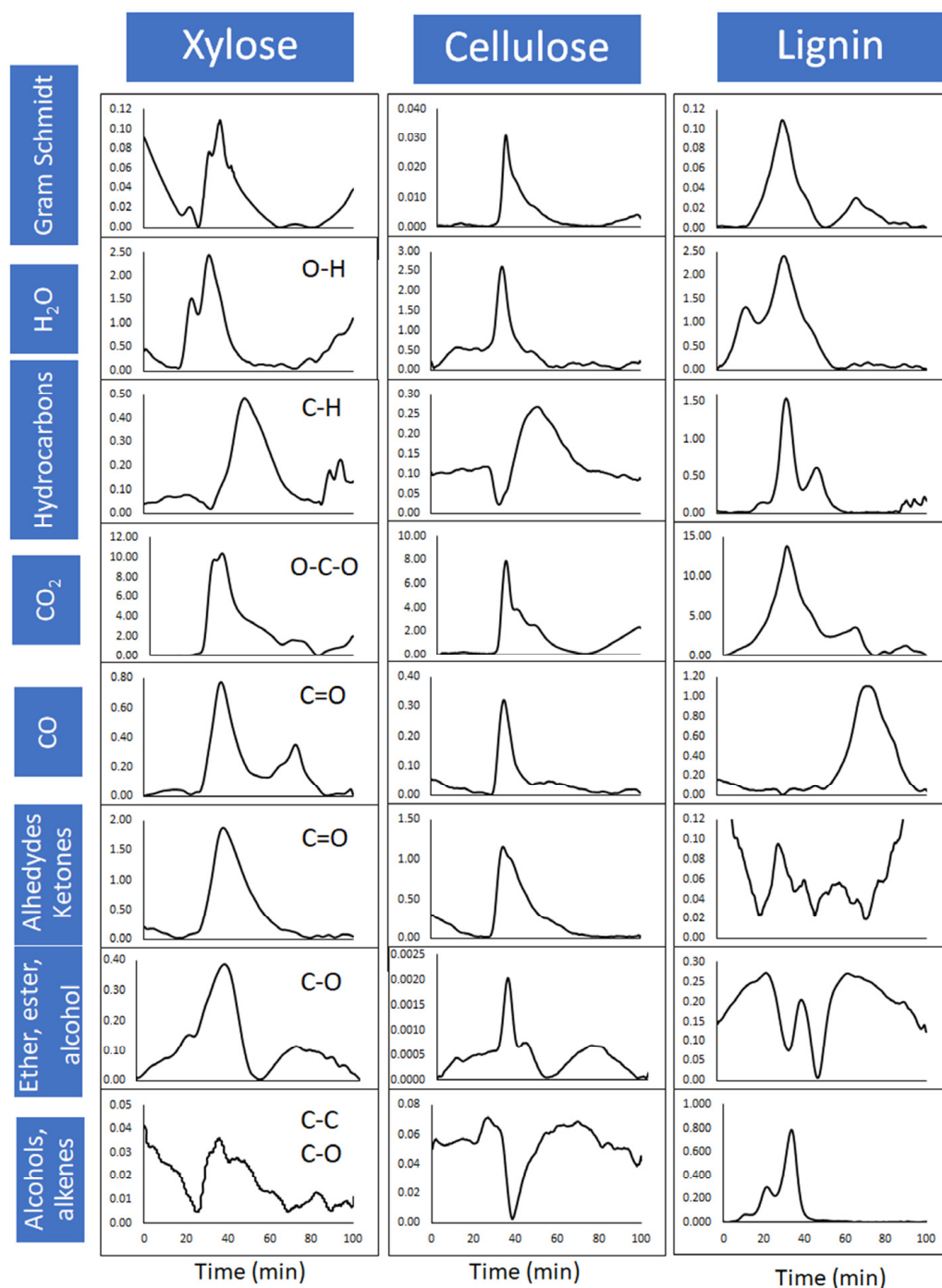


Figure 4. FT-IR spectra (chemigrams) of evolved gases during thermal decomposition of biomass constituents.

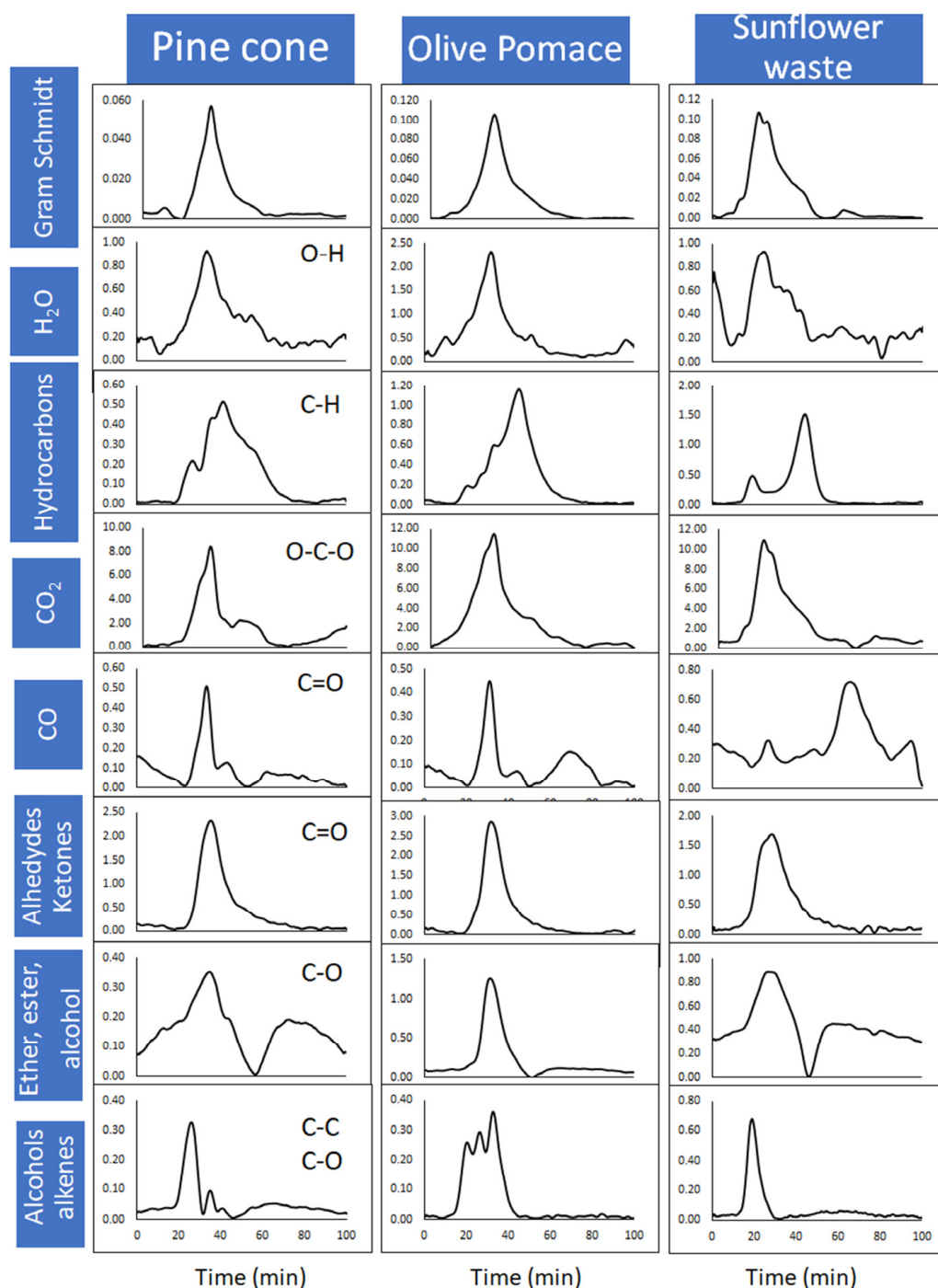


Figure 5. FT-IR spectra (chemigrams) of evolved gases during the thermal decomposition of biomass samples.

All biomass samples display noticeable chemigrams for CO₂, CH₄, and H₂O, as can be seen in Figure 5. The C-H vibrations of CH₄ evolution are detected between 19 and 74 min for pinecone pyrolysis as a single and wide-range peak. In contrast, sunflower waste produced CH₄ between 14 and 57 min with a two-step degradation. The first small peak at 18. minutes (~200 °C) is explained by the initialization reaction, and the second main peak at 43 min (~450 °C) is due to the final decomposition reactions of the holocellulosic fraction. These temperatures are in agreement with the TGA data (Table 4) and previous studies [58,62]. The release of aldehydes and/or ketones starts at 23, 20, and 14 min for pinecone, olive pomace, and sunflower, respectively. In addition, the

chemigrams illustrated for the wavelength between 1085–960 cm^{-1} , which are assigned to C-O stretching vibrations of alcohols and C-C stretching vibrations of alkenes, are viewed for all samples at different temperatures. All these differences in the evolved gas profiles demonstrate the effect of compositional differences in the samples and also the inexplicable synergetic effects of the combination of these natural polymers with inorganics arising from the ash content of biomass.

3.3. Pyrolysis Kinetics

The Coats–Redfern method was used to calculate pyrolysis kinetic parameters. The initial weight loss and removal of moisture from the biomass were not considered in the kinetic calculations. The decomposition of hemicellulose, cellulose, and lignin took place simultaneously in the pyrolysis process, exhibiting several parallel and series reactions [63]. From TGA-FTIR data (Gram–Schmidt curves), it is noticed that the degradation of xylose and lignin took place in three steps, while cellulose decomposed in one step.

The thermal degradation of xylose started at around 175 °C, being the component that decomposes in the first place at lower temperatures. The initial reactions required higher activation energies than the further decomposition reactions due to the elevated bond-breaking energies initially [64]. Cellulose decomposition demonstrated a rapid step between 290–350 °C, and the calculated activation energy is the highest among the other constituents. Similar results were reported previously for cellulose pyrolysis kinetic parameters by assuming a first-order degree decomposition [65]. A three-step decomposition scheme was recorded for the lignin degradation between the temperatures of 210–874 °C. The higher temperature decomposition reactions are assigned to char formation solidification reactions, and the calculated activation energy is lower than that of pyrolysis initialization reactions [66].

The activation energy required for the initiation of the thermal decomposition of biomass samples is in the range of 53–94 kJ/mol, which is close to that of xylose and lignin (Table 6). Since the selected biomass samples consist of similar holocellulose content, their initiation activation energies are close to each other. On the other hand, the kinetic calculation for the pinecone sample resulted in higher activation energy than that of olive pomace and sunflower waste. The low activation energies of sunflower waste prove that this biomass begins to decompose first compared to others, as explained before (Table 5). For all samples, it is seen that the initial pyrolysis reactions exhibited high activation energies, which could be unfavorable for the decomposition process. However, the higher pre-exponential factors calculated for the lower temperature decomposition zones indicated that the pyrolytic reactions were promoted. In other words, the compensating effect between activation energy and pre-exponential factor resulted in a stable overall reaction rate [67]. In addition, the R^2 values that are close to unity verify the first-order reaction assumption by yielding linear straight lines in the $\ln(g(\alpha)/T^2)$ versus $1/T$ graphics.

3.4. Pyrolysis Product Yields

Fixed bed pyrolysis reactor experiments were carried out with a 10 °C/min heating rate at the final temperature of 550 °C under 100 cm^3/min flow rate of nitrogen gas. Nitrogen gas was selected as the sweeping gas to prevent the formation of secondary reactions during devolatilization and increase the bio-oil yield, and also to maintain a similar atmosphere to TGA conditions [68]. The product yields distribution, which was calculated on a dry ash-free basis, is given in Figure 6. Bio-oil yields for biomass components could be listed from low to high as lignin, xylose, and cellulose. Although cellulose gave the highest bio-oil yield among the other constituents, 24.28 wt.% yield was significantly low when compared to lower temperature pyrolysis yields [69]. According to the data from TGA, the decomposition of cellulose was completed around 395 °C, and hence gas formation was enhanced at 550 °C final temperature rather than bio-oil. Having a high amount of volatile matter, the gaseous product yields were greater for xylose and cellulose, while the highly aromatic compound lignin yielded a relatively low gas product of 25.7 wt.%.

The water produced during the thermal degradation reactions of xylose draws attention in Figure 6. Since H₂O is one of the main products of possible pyrolysis reactions of xylose, 26.86 wt.% of water yield was achieved for this constituent [70]. On the other hand, 42.25 wt.% of char yield was recorded for lignin due to the charring reactions taking place at temperatures of higher than ~500 °C during lignin decomposition. In addition, the lowest bio-oil yield of 11.46 wt.% was achieved for lignin pyrolysis due to reconstruction, condensation, and polycondensation reactions occurring to form solid products rather than condensable volatiles. Also, the highly aromatic structure of lignin, which contains aromatic rings, makes it more thermally stable than the aliphatic bonds found in cellulose and hemicellulose. Since it is more difficult to break down these aromatic rings during pyrolysis, lignin produces fewer amounts of condensable volatiles, and hence the bio-oil yield is the lowest among the other constituents [43,71].

Table 6. Pyrolysis kinetic constants calculated by the Coats–Redfern method.

Sample	Temperature Range (°C)	E (kJ/mol)	A (1/min)	R ²
Xylose	173–249	104.57	5.700×10^9	0.8979
	258–355	52.13	6.560×10^3	0.9748
	360–690	10.11	0.106×10^1	0.9545
Cellulose	291–352	252.87	2.288×10^{21}	0.9989
	210–416	56.05	5.021×10^3	0.9614
Lignin	416–490	5.02	2.083×10^{-2}	0.9716
	672–874	24.28	0.421×10^1	0.9790
	188–350	52.80	3.110×10^4	0.9969
Olive pomace	350–410	25.81	0.310×10^1	0.9956
	410–535	15.05	0.130×10^1	0.9813
	210–310	93.52	3.960×10^8	0.9842
Pinecone	310–380	63.31	2.360×10^5	0.9841
	380–620	6.46	0.980×10^1	0.9910
	160–275	56.45	4.630×10^4	0.9880
Sunflower farm waste	275–380	24.66	1.990×10^1	0.9485
	380–520	8.94	0.060×10^1	0.9894

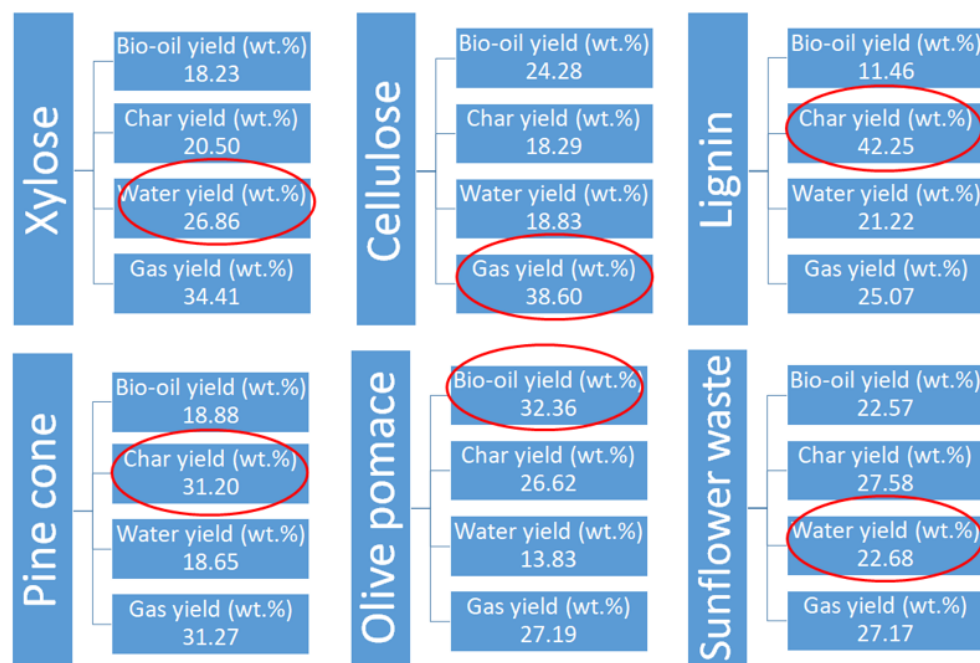


Figure 6. Slow pyrolysis product yields (heating rate: 10 °C/min, nitrogen flow rate: 100 mL/min).

The pyrolysis product yields of selected biomass samples are also given in Figure 6. Olive pomace yielded the highest amount of bio-oil (32.36 wt.%) when it is compared to other biomass samples. The lignin content of olive pomace was quite high, and hence lower bio-oil formation was expected due to the pyrolytic behavior of lignin, as explained above. However, the significant amount of n-hexane soluble oil content of olive pomace resulted in the condensable volatile formation through the possible complex reactions between -oic acids (mainly oleic acid) in the oil and lignocellulosic constituents. A woody plant—pinecone—had the lowest bio-oil yield of 18.88 wt.% and the highest char yield of 31.20 wt.% among the biomass samples. The lignin content of this forestry residue resulted in more charring reactions and, consequently, a high amount of char at the end of pyrolysis. Sunflower waste was characterized by its relatively high holocellulose content; therefore, the bio-oil and considerably high water yields were calculated to be around 22.6 wt.% and 22.7 wt.%, which lie in the range of agricultural waste pyrolysis yields [72,73]. Although the lignin content of sunflower waste was approximately 20 wt.%, the char yield was calculated to be close to that of olive pomace, which contained approximately 50% more lignin than sunflower waste. The reason for this elevated char yield could be explained by the ash content of sunflower waste. When compared to other samples, sunflower waste had the largest amount of inorganic content (ash) with 11.2 wt.%, and accordingly, the calculation using Equation (5) generated a higher char yield.

4. Conclusions

The effect of major components of lignocellulosic biomass on the pyrolytic behavior and as well as the slow pyrolysis bio-oil yield and composition, were investigated in this study. The following conclusions were derived from the experimental work:

- The highest decomposition rate was achieved at the temperatures of 305, 340, and 320 °C for xylose, cellulose, and lignin, respectively.
- Thermal decomposition of selected biomass samples showed similar behavior regardless of their different lignocellulosic structure and composition.
- The superimposition of hemicellulose, cellulose, and lignin degradation curves resulted in a three-step decomposition of biomass samples.
- The 3d visualization of evolved gases during pyrolysis demonstrates the steps of degradation through the gas products.
- The order of pyrolytic volatile production is hemicellulose (xylose), cellulose, and lignin, which is similar to their thermal decomposition and thermal stability.
- CO₂, CH₄, and H₂O are the main products of primary pyrolytic reactions such as cracking, reforming, and dehydration, whereas CO formation is accelerated at higher temperatures during the decomposition of lignin.
- Calculated activation energies revealed the fact that the initialization reactions required more energy than the secondary pyrolysis reactions, such as solidification and condensation.
- Laboratory-scale pyrolysis experiments yielded the highest amount of char for the highest lignin-containing biomass, whereas bio-oil formation was enhanced by the presence of high amounts of cellulose and hemicellulose. In addition, the highest bio-oil yield of 32.26 wt.% was obtained from olive oil pomace since it contains the highest n-hexane soluble fraction among the selected biomass samples.

As a result, it can be concluded that the major components of biomass have a significant effect on the decomposition rate and, accordingly, on the product yields and composition. However, other constituents of biomass, such as protein, ash, and extractives, also influence the quality of the bio-oil.

Author Contributions: Conceptualization, E.A.V.; methodology, E.A.V. and Ü.M.; investigation, Ü.M.; resources, E.A.V.; writing—original draft preparation, E.A.V. and Ü.M.; writing—review and editing, E.A.V.; visualization, E.A.V. and Ü.M.; supervision, E.A.V.; project administration, E.A.V. All authors have read and agreed to the published version of the manuscript.

Funding: This research was funded by Anadolu University Scientific Research Council, grant number 1110F166.

Data Availability Statement: Not applicable.

Acknowledgments: The contribution of COST Action LignoCOST (CA17128), supported by COST (European Cooperation in Science and Technology, www.cost.eu), in promoting interaction, exchange of knowledge, and collaborations in the field of lignin valorization is gratefully acknowledged.

Conflicts of Interest: The authors declare no conflict of interest. The funders had no role in the design of the study; in the collection, analyses, or interpretation of data; in the writing of the manuscript; or in the decision to publish the results.

References

1. Martins, F.; Felgueiras, C.; Smitkova, M.; Caetano, N. Analysis of Fossil Fuel Energy Consumption and Environmental Impacts in European Countries. *Energies* **2019**, *12*, 964. [[CrossRef](#)]
2. Sinsel, S.R.; Riemke, R.L.; Hoffmann, V.H. Challenges and Solution Technologies for the Integration of Variable Renewable Energy Sources—A Review. *Renew. Energy* **2020**, *145*, 2271–2285. [[CrossRef](#)]
3. Pang, S. Advances in Thermochemical Conversion of Woody Biomass to Energy, Fuels and Chemicals. *Biotechnol. Adv.* **2019**, *37*, 589–597. [[CrossRef](#)] [[PubMed](#)]
4. Rodionova, M.V.; Bozieva, A.M.; Zharmukhamedov, S.K.; Leong, Y.K.; Chi-Wei Lan, J.; Veziroglu, A.; Veziroglu, T.N.; Tomo, T.; Chang, J.S.; Allakhverdiev, S.I. A Comprehensive Review on Lignocellulosic Biomass Biorefinery for Sustainable Biofuel Production. *Int. J. Hydrogen Energy* **2022**, *47*, 1481–1498. [[CrossRef](#)]
5. McKendry, P. Energy Production from Biomass (Part 1): Overview of Biomass. *Bioresour. Technol.* **2002**, *83*, 37–46. [[CrossRef](#)]
6. Pasangulapati, V.; Ramachandriya, K.D.; Kumar, A.; Wilkins, M.R.; Jones, C.L.; Huhnke, R.L. Effects of Cellulose, Hemicellulose and Lignin on Thermochemical Conversion Characteristics of the Selected Biomass. *Bioresour. Technol.* **2012**, *114*, 663–669. [[CrossRef](#)]
7. Glasser, W.G. Lignin. In *Fundamentals of Thermochemical Biomass Conversion*; Overend, R.P., Milne, T.A., Mudge, L.K., Eds.; Springer: Dordrecht, The Netherlands, 1985; pp. 61–76. ISBN 978-94-009-4932-4.
8. Theander, O. Cellulose, Hemicellulose and Extractives. In *Fundamentals of Thermochemical Biomass Conversion*; Overend, R.P., Milne, T.A., Mudge, L.K., Eds.; Springer: Dordrecht, The Netherlands, 1985; pp. 35–60. ISBN 978-94-009-4932-4.
9. Mohan, D.; Pittman, C.U., Jr.; Steele, P.H. Pyrolysis of Wood/Biomass for Bio-oil: A Critical Review. *Energy Fuels* **2006**, *20*, 848–889. [[CrossRef](#)]
10. Wang, S.; Guo, X.; Wang, K.; Luo, Z. Influence of the interaction of components on the pyrolysis behavior of biomass. *J. Anal. Appl. Pyrolysis* **2011**, *91*, 183–189. [[CrossRef](#)]
11. Peters, B. Prediction of pyrolysis of pistachio shells based on its components hemicellulose, cellulose and lignin. *Fuel Process. Technol.* **2011**, *92*, 1993–1998. [[CrossRef](#)]
12. Rutkowski, P. Pyrolysis of cellulose, xylan and lignin with the K₂CO₃ and ZnCl₂ addition for bio-oil production. *Fuel Process. Technol.* **2011**, *92*, 517–522. [[CrossRef](#)]
13. Chen, D.; Cen, K.; Zhuang, X.; Gan, Z.; Zhou, J.; Zhang, Y.; Zhang, H. Insight into biomass pyrolysis mechanism based on cellulose, hemicellulose, and lignin: Evolution of volatiles and kinetics, elucidation of reaction pathways, and characterization of gas, biochar and bio-oil. *Combust. Flame* **2022**, *242*, 112142. [[CrossRef](#)]
14. Zhu, L.; Zhong, Z. Effects of cellulose, hemicellulose and lignin on biomass pyrolysis kinetics. *Korean J. Chem. Eng.* **2020**, *37*, 1660–1668. [[CrossRef](#)]
15. Yogalakshmi, K.N.; Poornima Devi, T.; Sivashanmugam, P.; Kavitha, S.; Yukesh Kannah, R.; Varjani, S.; AdishKumar, S.; Kumar, G.; Banu, J.R. Lignocellulosic Biomass-Based Pyrolysis: A Comprehensive Review. *Chemosphere* **2022**, *286*, 131824. [[CrossRef](#)]
16. Raveendran, K.; Ganesh, A.; Khilar, K.C. Pyrolysis Characteristics of Biomass and Biomass Components. *Fuel* **1996**, *75*, 987–998. [[CrossRef](#)]
17. Várhegyi, G.; Antal, M.J.; Jakab, E.; Szabó, P. Kinetic Modeling of Biomass Pyrolysis. *J. Anal. Appl. Pyrolysis* **1997**, *42*, 73–87. [[CrossRef](#)]
18. Orfão, J.J.M.; Antunes, F.J.A.; Figueiredo, J.L. Pyrolysis Kinetics of Lignocellulosic Materials—Three Independent Reactions Model. *Fuel* **1999**, *78*, 349–358. [[CrossRef](#)]
19. Koufopoulos, C.A.; Lucchesi, A.; Maschio, G. Kinetic Modelling of the Pyrolysis of Biomass and Biomass Components. *Can. J. Chem. Eng.* **1989**, *67*, 75–84. [[CrossRef](#)]
20. Bridgwater, A.V.; Meier, D.; Radlein, D. An Overview of Fast Pyrolysis of Biomass. *Org. Geochem.* **1999**, *30*, 1479–1493. [[CrossRef](#)]
21. Igliński, B.; Kujawski, W.; Kielkowska, U. Pyrolysis of Waste Biomass: Technical and Process Achievements, and Future Development—A Review. *Energies* **2023**, *16*, 1829. [[CrossRef](#)]
22. Abou Rjeily, M.; Cazier, F.; Gennequin, C.; Randrianalisoa, J.H. Detailed Analysis of Gas, Char and Bio-Oil Products of Oak Wood Pyrolysis at Different Operating Conditions. *Waste Biomass Valorization* **2023**, *14*, 325–343. [[CrossRef](#)]

23. Faleeva, Y.M.; Lavrenov, V.A.; Zaichenko, V.M. Investigation of Plant Biomass Two-Stage Pyrolysis Based on Three Major Components: Cellulose, Hemicellulose, and Lignin. *Biomass Convers. Biorefinery* **2022**. [CrossRef]
24. Mishra, R.K.; Mohanty, K. Pyrolysis Kinetics and Thermal Behavior of Waste Sawdust Biomass Using Thermogravimetric Analysis. *Bioresour. Technol.* **2018**, *251*, 63–74. [CrossRef] [PubMed]
25. Mishra, R.K.; Mohanty, K. Pyrolysis of Three Waste Biomass: Effect of Biomass Bed Thickness and Distance between Successive Beds on Pyrolytic Products Yield and Properties. *Renew. Energy* **2019**, *141*, 549–558. [CrossRef]
26. Gani, A.; Naruse, I. Effect of Cellulose and Lignin Content on Pyrolysis and Combustion Characteristics for Several Types of Biomass. *Renew. Energy* **2007**, *32*, 649–661. [CrossRef]
27. Klinger, J.L.; Westover, T.L.; Emerson, R.M.; Williams, C.L.; Hernandez, S.; Monson, G.D.; Ryan, J.C. Effect of Biomass Type, Heating Rate, and Sample Size on Microwave-Enhanced Fast Pyrolysis Product Yields and Qualities. *Appl. Energy* **2018**, *228*, 535–545. [CrossRef]
28. Abhijeet, P.; Swagathnath, G.; Rangabhashiyam, S.; Asok Rajkumar, M.; Balasubramanian, P. Prediction of Pyrolytic Product Composition and Yield for Various Grass Biomass Feedstocks. *Biomass Convers. Biorefin.* **2020**, *10*, 663–674. [CrossRef]
29. Tsekos, C.; Tandurella, S.; de Jong, W. Estimation of Lignocellulosic Biomass Pyrolysis Product Yields Using Artificial Neural Networks. *J. Anal. Appl. Pyrolysis* **2021**, *157*, 105180. [CrossRef]
30. Hoang, A.T.; Ong, H.C.; Fattah, I.M.R.; Chong, C.T.; Cheng, C.K.; Sakthivel, R.; Ok, Y.S. Progress on the Lignocellulosic Biomass Pyrolysis for Biofuel Production toward Environmental Sustainability. *Fuel Process. Technol.* **2021**, *223*, 106997. [CrossRef]
31. White, J.E.; Catallo, W.J.; Legendre, B.L. Biomass Pyrolysis Kinetics: A Comparative Critical Review with Relevant Agricultural Residue Case Studies. *J. Anal. Appl. Pyrolysis* **2011**, *91*, 1–33. [CrossRef]
32. Pütün, A.E.; Apaydm, E.; Pütün, E. Rice Straw as a Bio-Oil Source via Pyrolysis and Steam Pyrolysis. *Energy* **2004**, *29*, 2171–2180. [CrossRef]
33. Pütün, A.E.; Uzun, B.B.; Apaydin, E.; Pütün, E. Bio-Oil from Olive Oil Industry Wastes: Pyrolysis of Olive Residue under Different Conditions. *Fuel Process. Technol.* **2005**, *87*, 25–32. [CrossRef]
34. Cai, J.; He, Y.; Yu, X.; Banks, S.W.; Yang, Y.; Zhang, X.; Yu, Y.; Liu, R.; Bridgwater, A.V. Review of Physicochemical Properties and Analytical Characterization of Lignocellulosic Biomass. *Renew. Sustain. Energy Rev.* **2017**, *76*, 309–322. [CrossRef]
35. Fahmi, R.; Bridgwater, A.V.; Darvell, L.I.; Jones, J.M.; Yates, N.; Thain, S.; Donnison, I.S. The Effect of Alkali Metals on Combustion and Pyrolysis of Lolium and Festuca Grasses, Switchgrass and Willow. *Fuel* **2007**, *86*, 1560–1569. [CrossRef]
36. Yang, X.; Berglund, L.A. Structural and Ecofriendly Holocellulose Materials from Wood: Microscale Fibers and Nanoscale Fibrils. *Adv. Mater.* **2021**, *33*, 2001118. [CrossRef] [PubMed]
37. Akhtar, N.; Goyal, D.; Goyal, A. Physico-Chemical Characteristics of Leaf Litter Biomass to Delineate the Chemistries Involved in Biofuel Production. *J. Taiwan Inst. Chem. Eng.* **2016**, *62*, 239–246. [CrossRef]
38. Singh, S.B.; De, M. Thermally Exfoliated Graphene Oxide for Hydrogen Storage. *Mater. Chem. Phys.* **2020**, *239*, 122102. [CrossRef]
39. Md Salim, R.; Asik, J.; Sarjadi, M.S. Chemical Functional Groups of Extractives, Cellulose and Lignin Extracted from Native *Leucaena Leucocephala* Bark. *Wood Sci. Technol.* **2021**, *55*, 295–313. [CrossRef]
40. Kim Song, D. Le Libretext Chemistry. Available online: [https://chem.libretexts.org/Bookshelves/Physical_and_Theoretical_Chemistry_Textbook_Maps/Supplemental_Modules_\(Physical_and_Theoretical_Chemistry\)/Chemical_Bonding/Fundamentals_of_Chemical_Bonding/Bond_Energies#:~:text=A%20C%E2%80%93C%20bond%20has,of%20about%20145%20kcal%2Fmol](https://chem.libretexts.org/Bookshelves/Physical_and_Theoretical_Chemistry_Textbook_Maps/Supplemental_Modules_(Physical_and_Theoretical_Chemistry)/Chemical_Bonding/Fundamentals_of_Chemical_Bonding/Bond_Energies#:~:text=A%20C%E2%80%93C%20bond%20has,of%20about%20145%20kcal%2Fmol) (accessed on 30 March 2023).
41. Collard, F.X.; Blin, J. A Review on Pyrolysis of Biomass Constituents: Mechanisms and Composition of the Products Obtained from the Conversion of Cellulose, Hemicelluloses and Lignin. *Renew. Sustain. Energy Rev.* **2014**, *38*, 594–608. [CrossRef]
42. Yang, H.; Yan, R.; Chen, H.; Zheng, C.; Lee, D.H.; Liang, D.T. In-Depth Investigation of Biomass Pyrolysis Based on Three Major Components: Hemicellulose, Cellulose and Lignin. *Energy Fuels* **2006**, *20*, 388–393. [CrossRef]
43. Kawamoto, H. Lignin Pyrolysis Reactions. *J. Wood Sci.* **2017**, *63*, 117–132. [CrossRef]
44. Cao, J.; Xiao, G.; Xu, X.; Shen, D.; Jin, B. Study on Carbonization of Lignin by TG-FTIR and High-Temperature Carbonization Reactor. *Fuel Process. Technol.* **2013**, *106*, 41–47. [CrossRef]
45. Yang, H.; Yan, R.; Chen, H.; Lee, D.H.; Zheng, C. Characteristics of Hemicellulose, Cellulose and Lignin Pyrolysis. *Fuel* **2007**, *86*, 1781–1788. [CrossRef]
46. Caballero, J.A.; Conesa, J.A.; Font, R.; Marcilla, A. Pyrolysis Kinetics of Almond Shells and Olive Stones Considering Their Organic Fractions. *J. Anal. Appl. Pyrolysis* **1997**, *42*, 159–175. [CrossRef]
47. Coker, E.N.; Lujan-Flores, X.; Donaldson, B.; Yilmaz, N.; Atmanli, A. An Assessment of the Conversion of Biomass and Industrial Waste Products to Activated Carbon. *Energies* **2023**, *16*, 1606. [CrossRef]
48. Escalante, J.; Chen, W.H.; Tabatabaei, M.; Hoang, A.T.; Kwon, E.E.; Andrew Lin, K.Y.; Saravanakumar, A. Pyrolysis of Lignocellulosic, Algal, Plastic, and Other Biomass Wastes for Biofuel Production and Circular Bioeconomy: A Review of Thermogravimetric Analysis (TGA) Approach. *Renew. Sustain. Energy Rev.* **2022**, *169*, 112914. [CrossRef]
49. Emiola-Sadiq, T.; Zhang, L.; Dalai, A.K. Thermal and Kinetic Studies on Biomass Degradation via Thermogravimetric Analysis: A Combination of Model-Fitting and Model-Free Approach. *ACS Omega* **2021**, *6*, 22233–22247. [CrossRef]
50. Olatunji, O.O.; Akinlabi, S.A.; Mashinini, M.P.; Fatoba, S.O.; Ajayi, O.O. Thermo-Gravimetric Characterization of Biomass Properties: A Review. *IOP Conf. Series Mater. Sci. Eng.* **2018**, *423*, 12175. [CrossRef]

51. Akhtar, J.; Imran, M.; Ali, A.M.; Nawaz, Z.; Muhammad, A.; Butt, R.K.; Jillani, M.S.; Naeem, H.A. Torrefaction and Thermochemical Properties of Agriculture Residues. *Energies* **2021**, *14*, 4218. [[CrossRef](#)]
52. Fasina, O.; Littlefield, B. TG-FTIR Analysis of Pecan Shells Thermal Decomposition. *Fuel Process. Technol.* **2012**, *102*, 61–66. [[CrossRef](#)]
53. Qu, T.; Guo, W.; Shen, L.; Xiao, J.; Zhao, K. Experimental Study of Biomass Pyrolysis Based on Three Major Components: Hemicellulose, Cellulose, and Lignin. *Ind. Eng. Chem. Res.* **2011**, *50*, 10424–10433. [[CrossRef](#)]
54. Apaydin-Varol, E.; Uzun, B.B.; Önal, E.; Pütün, A.E. Synthetic Fuel Production from Cottonseed: Fast Pyrolysis and a TGA/FT-IR/MS Study. *J. Anal. Appl. Pyrolysis* **2014**, *105*, 83–90. [[CrossRef](#)]
55. Wu, Y.-M.; Zhao, Z.-L.; Li, H.-B.; He, F. Low Temperature Pyrolysis Characteristics of Major Components of Biomass. *J. Fuel Chem. Technol.* **2009**, *37*, 427–432. [[CrossRef](#)]
56. Schindler, A.; Neumann, G.; Rager, A.; Füglein, E.; Blumm, J.; Denner, T. A Novel Direct Coupling of Simultaneous Thermal Analysis (STA) and Fourier Transform-Infrared (FT-IR) Spectroscopy. *J. Therm. Anal. Calorim.* **2013**, *113*, 1091–1102. [[CrossRef](#)]
57. Yıldız, Z.; Ceylan, S. Pyrolysis of Tobacco Factory Waste Biomass. *J. Therm. Anal. Calorim.* **2019**, *136*, 783–794. [[CrossRef](#)]
58. Fu, P.; Hu, S.; Xiang, J.; Li, P.; Huang, D.; Jiang, L.; Zhang, A.; Zhang, J. FTIR Study of Pyrolysis Products Evolving from Typical Agricultural Residues. *J. Anal. Appl. Pyrolysis* **2010**, *88*, 117–123. [[CrossRef](#)]
59. Ma, Z.; Chen, D.; Gu, J.; Bao, B.; Zhang, Q. Determination of Pyrolysis Characteristics and Kinetics of Palm Kernel Shell Using TGA–FTIR and Model-Free Integral Methods. *Energy Convers. Manag.* **2015**, *89*, 251–259. [[CrossRef](#)]
60. Özsin, G.; Pütün, A.E. TGA/MS/FT-IR Study for Kinetic Evaluation and Evolved Gas Analysis of a Biomass/PVC Co-Pyrolysis Process. *Energy Convers. Manag.* **2019**, *182*, 143–153. [[CrossRef](#)]
61. Guo, X.J.; Wang, S.R.; Wang, K.G.; Liu, Q.; Luo, Z.Y. Influence of Extractives on Mechanism of Biomass Pyrolysis. *J. Fuel Chem. Technol.* **2010**, *38*, 42–46. [[CrossRef](#)]
62. Singh, S.; Wu, C.; Williams, P.T. Pyrolysis of Waste Materials Using TGA-MS and TGA-FTIR as Complementary Characterisation Techniques. *J. Anal. Appl. Pyrolysis* **2012**, *94*, 99–107. [[CrossRef](#)]
63. Alvarado Flores, J.J.; Alcaraz Vera, J.V.; Ávalos Rodríguez, M.L.; López Sosa, L.B.; Rutiaga Quiñones, J.G.; Pintor Ibarra, L.F.; Márquez Montesino, F.; Aguado Zarraga, R. Analysis of Pyrolysis Kinetic Parameters Based on Various Mathematical Models for More than Twenty Different Biomasses: A Review. *Energies* **2022**, *15*, 6524. [[CrossRef](#)]
64. Lei, Z.; Wang, S.; Fu, H.; Gao, W.; Wang, B.; Zeng, J.; Xu, J. Thermal Pyrolysis Characteristics and Kinetics of Hemicellulose Isolated from Camellia Oleifera Shell. *Bioresour. Technol.* **2019**, *282*, 228–235. [[CrossRef](#)]
65. Zhu, G.; Zhu, X.; Xiao, Z.; Yi, F. Study of Cellulose Pyrolysis Using an in Situ Visualization Technique and Thermogravimetric Analyzer. *J. Anal. Appl. Pyrolysis* **2012**, *94*, 126–130. [[CrossRef](#)]
66. Chen, L.; Hu, J.; Han, Q.; Xie, A.; Zhou, Z.; Yang, J.; Tang, Q.; Mi, B.; Wu, F. Application of Distributed Activation Energy Model and Coats-Redfern Integration Method in the Study of Industrial Lignin Pyrolysis Kinetics. *Biomass Convers. Biorefin.* **2022**. [[CrossRef](#)]
67. Mian, I.; Li, X.; Jian, Y.; Dacres, O.D.; Zhong, M.; Liu, J.; Ma, F.; Rahman, N. Kinetic Study of Biomass Pellet Pyrolysis by Using Distributed Activation Energy Model and Coats Redfern Methods and Their Comparison. *Bioresour. Technol.* **2019**, *294*, 122099. [[CrossRef](#)] [[PubMed](#)]
68. Slezak, R.; Unyay, H.; Szufa, S.; Ledakowicz, S. An Extensive Review and Comparison of Modern Biomass Reactors Torrefaction vs. Biomass Pyrolyzers—Part 2. *Energies* **2023**, *16*, 2212. [[CrossRef](#)]
69. Gao, Z.; Li, N.; Yin, S.; Yi, W. Pyrolysis Behavior of Cellulose in a Fixed Bed Reactor: Residue Evolution and Effects of Parameters on Products Distribution and Bio-Oil Composition. *Energy* **2019**, *175*, 1067–1074. [[CrossRef](#)]
70. Huang, J.; He, C.; Wu, L.; Tong, H. Thermal Degradation Reaction Mechanism of Xylose: A DFT Study. *Chem. Phys. Lett.* **2016**, *658*, 114–124. [[CrossRef](#)]
71. Lu, X.; Gu, X. A Review on Lignin Pyrolysis: Pyrolytic Behavior, Mechanism, and Relevant Upgrading for Improving Process Efficiency. *Biotechnol. Biofuels Bioprod.* **2022**, *15*, 106. [[CrossRef](#)]
72. Alper, K.; Tekin, K.; Karagöz, S. Pyrolysis of Agricultural Residues for Bio-Oil Production. *Clean Technol. Env. Policy* **2015**, *17*, 211–223. [[CrossRef](#)]
73. Hawash, S.I.; Farah, J.Y.; El-Diwani, G. Pyrolysis of Agriculture Wastes for Bio-Oil and Char Production. *J. Anal. Appl. Pyrolysis* **2017**, *124*, 369–372. [[CrossRef](#)]

Disclaimer/Publisher’s Note: The statements, opinions and data contained in all publications are solely those of the individual author(s) and contributor(s) and not of MDPI and/or the editor(s). MDPI and/or the editor(s) disclaim responsibility for any injury to people or property resulting from any ideas, methods, instructions or products referred to in the content.